Electrochemical investigation and thermodynamic assessment of the Mg-Pd system

W. Gierlotka[1*], S. Terlicka[2], W. Gąsior[2], A. Dębski[2], M. Pęska[3], M. Polański[3]

[1] National Dong Hwa University, Materials Science and Engineering Department, Hualien,

Taiwan

*e-mail: wojtek@gms.ndhu.edu.tw

[2] Institute of Metallurgy and Materials Science, Polish Academy of Sciences,

25 Reymonta Street, 30-059 Kraków, Poland

[3] Military University of Technology, 2 Kaliskiego Street, 00-908 Warsaw, Poland

Abstract

This work presents the results of electromotive force measurements, by coulometric titration technique, for liquid and solid Mg-Pd alloys with concentrations up to 0.70 mole fraction of Mg and at 918 K. These measurements enabled verification of the range of homogeneity of the occurring phases and phase boundaries in the studied system.

Based on the obtained results and other thermodynamic data found in the literature, the phase diagram of the Mg-Pd system was optimized using the CALPHAD method and ab initio calculations. The thermodynamics of intermetallic phases, liquid phase, and solid solutions were described by the proper equations which can be used in the future to calculate the multicomponent systems with the Mg-Pd system as one of the binary components. The thermodynamic calculations successfully reproduced the Mg-Pd phase diagram.

1 Introduction

Today, magnesium and its alloys are intensively studied in many industrial sectors, especially in the energy, automotive, and aerospace sectors, due to their good performance characteristics (including low density and high strength-to-weight ratio). However, due to the high reactivity of magnesium and magnesium-related materials with air constituents (especially at elevated temperatures), as well as the high vapor pressure of Mg at temperatures near (or above) the melting point of Mg, the thermodynamic and physicochemical properties of Mg and its alloys are not fully understood.

The literature information on the phase diagram of the Mg – Pd system is very limited. It is impossible to find a complex description of the phase equilibrium in this system. The first assessment of the Mg-Pd phase diagram was presented by Nayeb-Hashemi and Clark [1] who used differential thermal analysis (DTA), hardness, density, metallography, and X-ray diffraction analysis (XRD) data reported by Savitsky et al. [2] as well as reported by Ferro and Rambaldi [3] metallography and XRD findings. The phase diagram proposed by Nayeb-Hashemi and Clark is shown in Figure 1a. Savitsky et al. [2] originally postulated the presence of the Mg_2Pd_3 intermetallic phase, asserting its congruent melting point at 1350°C. Ferro and Rambaldi [3] findings revealed that the maximum solid solubility of Mg in Pd extends up to 25 atomic % Mg. Westen [4], in contrast to Ferro and Rambaldi [3], initial claim of the $Mg_{2.7}Pd$ intermetallic phase, introduced the nonstoichiometric phase Mg_5Pd_2, exhibiting a homogeneity range spanning from 25 to 28.56 atomic % Pd. Kripyakevich and Gladyshevskii [5] reported the presence of both MgPd (with a certain homogeneity range) and $Mg_{0.9}Pd_{1.1}$ intermetallic phases. Questioning the existence of the Mg_2Pd_3 compound due to insufficient evidence, Nayeb-Hashemi and Clark [1] suggested that the $Mg_{0.9}Pd_{1.1}$ phase might serve as a more plausible candidate for the intermetallic phase around 50 atomic % Pd. In 2006, Makongo et al. [6] presented a comprehensive Mg-Pd phase diagram, covering the range concentration from 0 to 56 atomic % Pd. Their results were derived from various analyses, including X-ray

spectroscopy, differential thermal analysis, and differential scanning calorimetry. Subsequently, building upon the findings of Nayeb-Hashemi and Clark [1] and Makongo et al. [6], Okamoto [7] provided an updated rendition of the Mg-Pd phase diagram, which is depicted in Figure 1b.
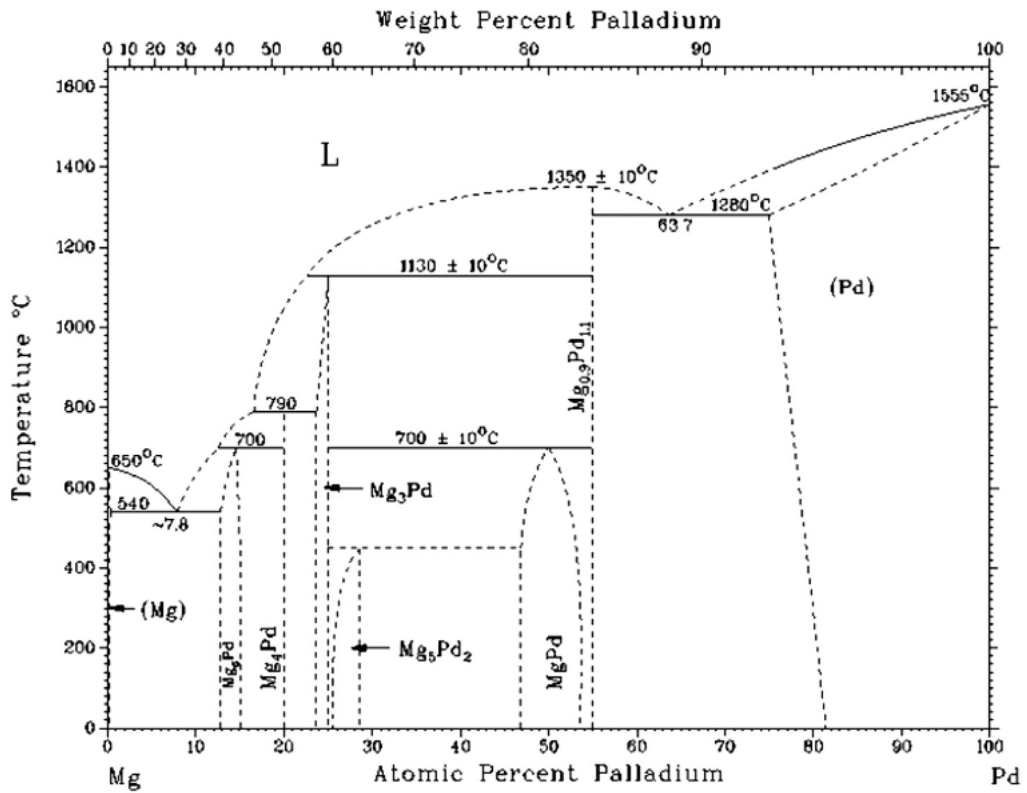
Figure 1a. A phase diagram of the Mg-Pd system proposed by Nayeb-Hashemi and Clark [1].
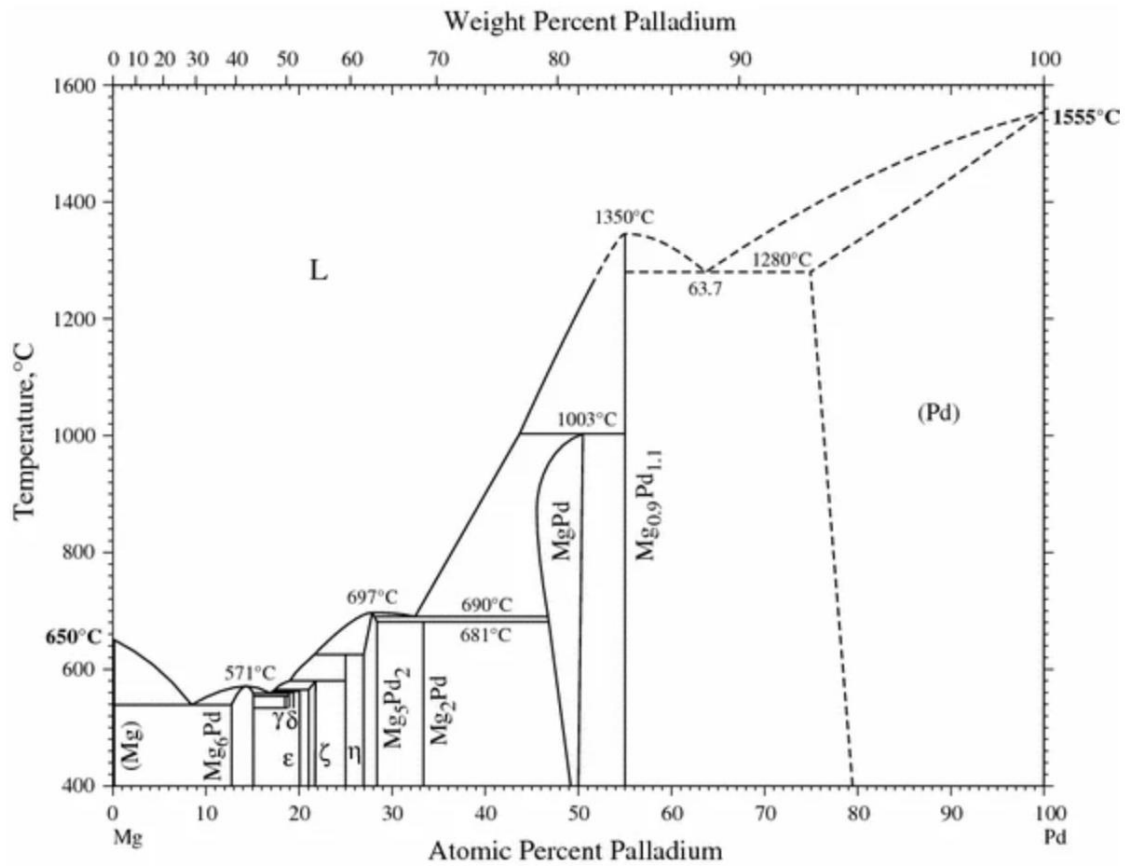
Figure 1b. A phase diagram of the Mg-Pd system proposed by Okamoto [7].

The Pd-rich part of the phase diagram was investigated by Eisheh [8]. Based on electromotive force measurement and diffusion couples analysis Eisheh [8] proposed phase equilibria for the composition of Pd greater than 0.5 mole fraction. In that proposition, phase $Mg_{0.9}Pd_{1.1}$ is not presented. Instead, there is the Mg_3Pd_5 phase. Moreover, the following phases are presented: $MgPd_3$ and $MgPd_2$ decompose by peritectic reactions at 977 and 901 K, respectively. Eisheh [8] also included a phase Mg_2Pd_5; however, the thermal stability of this compound is unknown.

Thermodynamic investigation on the formation enthalpy of intermetallic compounds includes Eisheh [8] work with data for $MgPd_3$, Mg_2Pd_5, $MgPd_2$, Mg_3Pd_5, as well, as MgPd. This work also provided formation enthalpy for the Mg_2Pd_3 phase, but that value is marked as a value for non-stoichiometric Mg_3Pd_5. All enthalpies of formation given by Eisheh [8] were

4

measured at 1073 K. Delsante et al. [9] measured the formation enthalpy of the Mg_6Pd, and Mg_5Pd_2 phases. In addition, four samples with compositions equal to 0.29, 0.16, 0.135, and 0.125 mole fraction of Pd were examined by differential scanning calorimeter (DSC). Debski et al. [10] measured the formation enthalpy for alloys containing respectively: 14.6 at.% Pd (Mg_6Pd), 19.4 at.% Pd (~Mg_4Pd or ε phase), 20.1 at.% Pd (~ζ phase), 27.7 at.% Pd (~Mg_3Pd or η phase), 29.3 at.% Pd (Mg_5Pd_2 phase), and 35.5 at.% Pd (~Mg_2Pd phase). The results obtained for Mg_6Pd show a similar heat effect to Delsante et al. [9] results, and the formation enthalpy of the Mg_5Pd_2 phase determined by Dębski et al. [10] exhibits more negative values than those presented by Delsante et al. [9]. Mixing enthalpy of liquid was measured by Dębski et al. [10] in the concentration range up to 0.24 mole fraction of Pd at 990, and 1031 K.

The formation energies and bulk modulus of intermetallic compounds in the Mg-Pd system were determined by ab initio method by Gierlotka et al. [11]. To the best knowledge of the authors, the literature does not provide information on the experimental determination of the properties calculated in the mentioned above work [11].

Since there is no thermodynamic description of the binary Mg-Pd system, so the main aim of this work was to provide the calculations of phase equilibrium in the Mg-Pd system and present the set of equations describing the thermodynamics of phase. Moreover, electrochemical measurements of the Mg-Pd system down to 0.7 molar fraction of Mg have not been performed before, so additionally, this work presents such measurements as a continuation of our previous studies [12], [10], [13]. Based on electrochemical data obtained in this work and our previous experimental values studies [12], [10], [13], as well as on the phase diagram, thermochemical and structural data available in the literature, the first complete thermodynamic assessment of the Mg-Pd system using the CALPHAD method is given.

2   Experimental

2.1   Electromotive force studies (EMF) – coulometric titration method

Coulometric titration enables the determination of the dependence of the electromotive force (E) on the concentration of magnesium (x_{Mg}) at a constant temperature. In this method, the cells are heated to a selected temperature and then, after a stable temperature and electromotive force values, a current is passed through the cell for a specified time [14], [15], [16], [17]. The concentration of Mg in the alloy under test is determined based on Faraday's first and second laws of electrolysis.

The electrochemical concentration cell method was applied to study the thermodynamic properties of the Mg-Pd system. The scheme of the concentration cell used for the coulometric titration method for alloys from the Mg-Pd system can be represented below (1) and the construction of the measuring cell is shown in Fig. 2.

$$Mg_{(s)} \big| LiCl - LiF - MgCl_2 \ elctrolyte_{(l)} \big| Pd_{(s)} \tag{1}$$
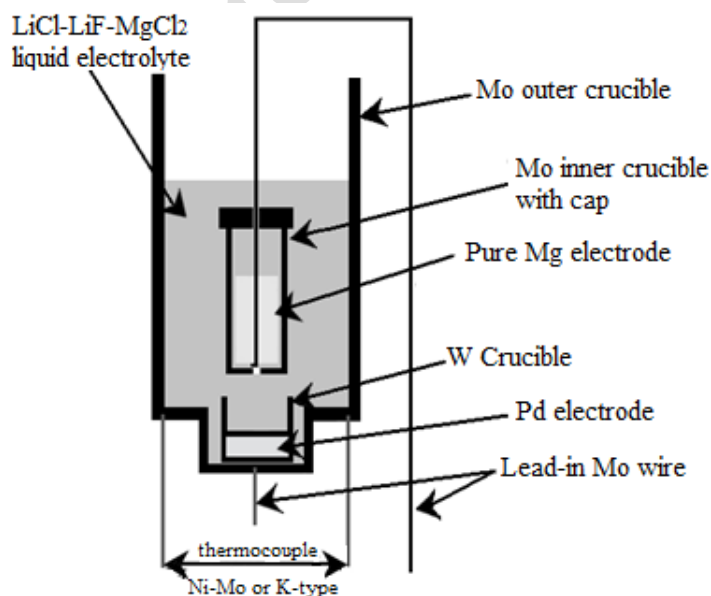
Figure 2. Scheme of the measuring cell used in the study of the electromotive force of alloys from the Mg-Pd system.

Pure magnesium was used as a reference electrode, which before each measurement was carefully, mechanically cleaned with a file to remove surface contaminants and then drilled

through the center obtaining a hole in which a molybdenum lead-in wire was placed. As an electrolyte a eutectic mixture of LiCl-LiF salts with the addition of 5 % at. Anhydrous $MgCl_2$ salt was used. It was prepared by mixing appropriate amounts of pure LiCl, LiF, and $MgCl_2$ salts in a quartz tube and melting them in a resistance furnace. Subsequently, hydrogen chloride gas was purged through the liquid salts to remove impurities, (i.e., water or Li salt carbonates) after which Ar was bubbled through the molten salts to remove traces of absorbed HCl. Then, the electrolytic salts prepared in this way (still hot and liquid) were introduced into a glove box (mBraun) to protect them from absorbing moisture from the atmosphere.

For electrochemical measurement of the Mg-Pd system, pure Pd wire (from about 0.10 to 0.20 g) was used, which before the measurement was rolled and pressed using a hydraulic press in order to obtain a homogeneous plate with a diameter of about 10 mm. Next, the obtained small disk was annealed in a glove box with a protective atmosphere at a temperature of c.a. 800 °C for 4 hours. The Pd sample prepared in this way was placed in a tungsten crucible in the measuring cell.

All cell components were carefully cleaned before assembly, the electrolyte was ground in an electric mill to obtain a homogeneous powder. Moreover, the cell for electromotive force measurements was assembled in a glove box with a high-purity Ar protective atmosphere [18], [19]. The characterization of used materials in the EMF measurements is collected in Table 1.

Table 1. Specification of applied materials.

Chemical name	Source	Purity [wt. %]	Form	Analysis method
Magnesium	Sigma Aldrich	99.9	Rod	Certified purity
Palladium	Safina a.s.	99.95	Wire	Certified purity
Lithium chloride anhydrous	Alfa Aesar	99	Powder	Certified purity
Lithium fluoride	Alfa Aesar	98	Powder	Certified purity

Magnesium chloride anhydrous	Alfa Aesar	99	Powder	Certified purity
Argon	Air Products	99.9999	Gas	Certified purity

2.2 *Calculations*

In this study, we primarily employed the ab initio method, a cornerstone of density functional theory (DFT), as implemented in VASP [20], for most of our computational tasks. The calculations relied on the general gradient approximation (GGA) pseudopotential, parameterized according to Perdew, Burke, and Ernzerhof's specifications [21]. To model interactions between ions and electrons, we adopted the projector augmented wave (PAW) approach [20], with the valence electron configurations being s2p0 for Mg and s1d9 for Pd.

In terms of computational parameters, we set the cut-off energy to 400 eV and utilized a gamma-centered mesh grid with a density of 0.09 A^-1. The choice of a cut-off energy exceeding 1.3 times the maximum specified in the pseudopotential file was consistent with guidelines for phonon calculations [22]. Our selected mesh grid density ensured convergence with calculations differing by less than 1 meV.

For self-consistent electronic loop calculations, we established a break-up condition of 10^-9. Regarding structural relaxation, we employed the conjugate gradient algorithm [23] with break-up conditions set at 10^-4 eV/A, striking an optimal balance between precision and computational efficiency. Furthermore, we enabled the ADDGRID tag during the calculations, providing additional support for the evaluation of augmentation charges.

Formation energies of intermetallic compounds were calculated in accordance with Equation 2.

$$\Delta E_{Mg_nPd_m} = E_{Mg_nPd_m} - \frac{n}{n+m}E_{Mg} - \frac{m}{n+m}E_{Pd} \tag{2}$$

where $\Delta E_{Mg_nPd_m}$ is formation energy, $E_{Mg_nPd_m}$, E_{Mg}, E_{Pd} are energies of the intermediate phase, Mg in HCP_A3 structure, and Pd in FCC_A1 structure, respectively.

We computed the temperature-dependent variations in thermodynamic properties as a function of temperature by applying the Helmholtz energy equation, following the stepwise procedure outlined below.

It is known that the Helmholtz energy, which is a function of volume and temperature, is the sum of three kinds of energies and is given as follows:

$$F(V,T) = E_c(V) + F_{ph}(V,T) + F_{el}(V,T) \tag{3}$$

where $F(V,T)$ is the Helmholtz energy, $E_c(V)$ is the energy of the crystal obtained from the self-consistent field (SCF) calculation at 0 K, $F_{ph}(V,T)$ is the vibrational free energy of ions, and $F_{el}(V,T)$ is the electronic free energy.

The vibrational free energy $F_{ph}(V,T)$ can be obtained from the quasi-harmonic approximation [24]:

$$F_{ph}(V,T) = k_B T \sum_q \sum_j \ln\left\{2\sinh\left[\frac{\hbar\omega_j(q,V)}{2k_BT}\right]\right\} \tag{4}$$

where k_B is the Boltzmann constant, T is absolute temperature, $\hbar$ is Planck's constant divided by 2π, and $\omega_j(q,V)$ is the frequency of the j-th phonon mode at wave vector q.

The electronic contribution to the Helmholtz energy is calculated from the following equations, which describe the dependence of different energies on temperature and volume:

$$F_{el}(V,T) = E_{el}(V,T) - TS_{el}(V,T) \tag{5}$$

$$S_{el}(V,T) = -k_B \int n(\varepsilon,V)[f\ln f + (1-f)\ln(1-f)]d\varepsilon \tag{6}$$

$$E_{el}(V,T) = \int n(\varepsilon,V)f\varepsilon\,d\varepsilon - \int^{\varepsilon_F} n(\varepsilon,V)\varepsilon\,d\varepsilon \tag{7}$$

where $F_{el}(V,T)$ is the electronic Helmholtz energy, $S_{el}(V,T)$ is the electronic entropy, $E_{el}(V,T)$ is the electronic energy, $n(\varepsilon,V)$ is the electronic density of states, ε_F is the energy of the Fermi level, and f is the Fermi distribution.

To determine the Helmholtz energy using Eqs 4-7, the Phonopy code was used in the calculation starting from the determination of atomic forces from finite displacements. In the next step, cells with slightly different volumes (larger and smaller than the equilibrium volume) were defined, and the calculations were repeated. After this procedure, it was possible to determine mode Grüneisen parameters, and with the use of the quasi-harmonic approximation [24], properties such as isobaric heat capacity and Gibbs energies as functions of temperature were determined.

The final task in this study involved the prediction of a phase diagram for the Mg-Pd system using the Calphad approach [25]. The Calphad method enjoys broad application across various domains within materials science [26], [27], [28], making it a fitting choice for addressing the particular issue at hand. In our analysis, the thermodynamic description of the magnesium-platinum system encompassed the following phases: Liquid, HCP_A3(Mg), FCC_A1(Pd), Mg_6Pd, $Mg_{306}Pd_{77}$ (ε), $Mg_{785}Pd_{215}$ (ζ), Mg_3Pd (η), Mg_5Pd_2, Mg_2Pd, MgPd, $Mg_{0.9}Pd_{1.1}$, $MgPd_2$, and $MgPd_3$. The liquid and FCC_A1(Pt) phases were described by a substitutional model whereas other phases were treated as stoichiometric compounds.

The Gibbs free energies of pure elements with respect to temperature $^0G_i(T) = G_i(T) - H_i^{SER}$ are represented by Equation 8:

$$^0G_i(T) = a + bT + cT\ln(T) + dT^2 + eT^{-1} + fT^3 + iT^4 + jT^7 + kT^{-9} \qquad (8)$$

The $^0G_i(T)$ data have been standardized concerning the constant enthalpy value of the reference standard element H_i^{SER} at 298.15 K and 1 bar, according to the recommendations of the Scientific Group Thermodata Europe (SGTE) [29]. The reference states for this standardization are HCP_A3 for magnesium and FCC_A1 for palladium. The expression for $^0G_i(T)$ can vary across different temperature ranges, with coefficients a, b, c, d, e, f, I, j, and k taking on distinct values. These $^0G_i(T)$ functions are sourced from the SGTE Unary (Pure elements) TDB v.5. [29].

The Liquid and FCC_A1(Pt) phases were described by the substitutional solution model and their Gibbs energies are given as follows:

$$^mG_{Mg,Pd}^{\alpha} = x_{Mg}\ {}^0G_{Mg}^{\alpha} + x_{Pd}\ {}^0G_{Pd}^{\alpha} + RT\big(x_{Mg}lnx_{Mg} + x_{Pd}lnx_{Pd}\big) + x_{Mg}x_{Pd}\sum_i\ {}^iL_{Mg,Pd}^{\alpha}$$

(9)

where R is the gas constant, T is the absolute temperature, ${}^iL_{Mg,Pd}^{\alpha}$ are adjustable parameters, and i is an integer (i = 0, 1, 2…), α is a phase (α = Liquid, FCC_A1(Pd)), the adjustable ${}^iL_{Mg,Pd}^{\alpha}$ parameters are coefficient of the Redlich-Kister polynomial that is used for describing the excess Gibbs energy.

All the other phases were described as stoichiometric compounds, and their Gibbs energies were modeled as follows:

$$^0G_{Mg:Pd}^{Mg_mPd_n} = a + bT + cTln(T) + m*GHSERMG + n*GHSERPD$$ (10)

where a, b, c, are adjustable parameters, T is the absolute temperature, m, n are the stoichiometric coefficients, and *GHSERMG* and *GHSERPD* are the Gibbs energies of Mg and Pd in their Standard Element Reference (SER) state, respectively.

The magnesium was treated as a pure element due to the negligible solubility of Pd in Mg.

3   Results and discussion

3.1   *Results of the electromotive force measurements analysis*

The coulometric titration method allows to determination of the range of homogeneity of the phases present and the phase boundaries in the system under study, because the values of E in the two-phase regions are constant and independent of the component concentration, while in the one-phase region the values of E change with concentration [14], [15], [16], [17].

Coulometric titration measurements were carried out using a constant current of 1 mA (0.001 A) and a variable electrical pulse time ranging from 1200 s to 7200 s. Coulometric titrations in the Mg-Pd system were performed at 918 K.

Because the reference (pure Mg) and simultaneously working electrode in the applied temperature range was solid, the waiting time for the system to return to equilibrium after each set electrical pulse was long ranging from 3600 s to more than 54 000 s and depended on the applied temperature (the higher the temperature the faster the system returned to equilibrium after the set pulse) and the Mg concentration (the higher the Mg concentration in the formed alloy the slower the system returned to equilibrium). The long relaxation time of the sample was due to the very slow diffusion of magnesium atoms from the surface of the Pd (Mg-Pd) plate to the bulk and thus the slow formation of intermetallic phases and phase regions in the sample.

Electrochemical measurement was carried out up to a maximum magnesium content of approximately 0.7 mole fraction of Mg. Unfortunately, due to the high evaporation of magnesium at elevated temperatures and the reaction of magnesium vapor with the quartz tube used as a cover for the measuring cell, not all of the coulometric titration measurements could be performed up to a content of $x_{Mg}= 0.70$.

Figure 3 presents the coulometric titration curve for the Mg-Pd system at 918 K. A large range of solubility of magnesium in palladium is visible up to c.a. 0.18 mole fraction of Mg. Then, there are several more or less visible characteristic jumps in the electromotive force values within the x_{Mg} values corresponding, according to the available literature [1], [6], [8], to intermetallic phases of the following order: $MgPd_3$, $MgPd_2$, $Mg_{0.9}Pd_{1.1}$, $MgPd$, Mg_2Pd.
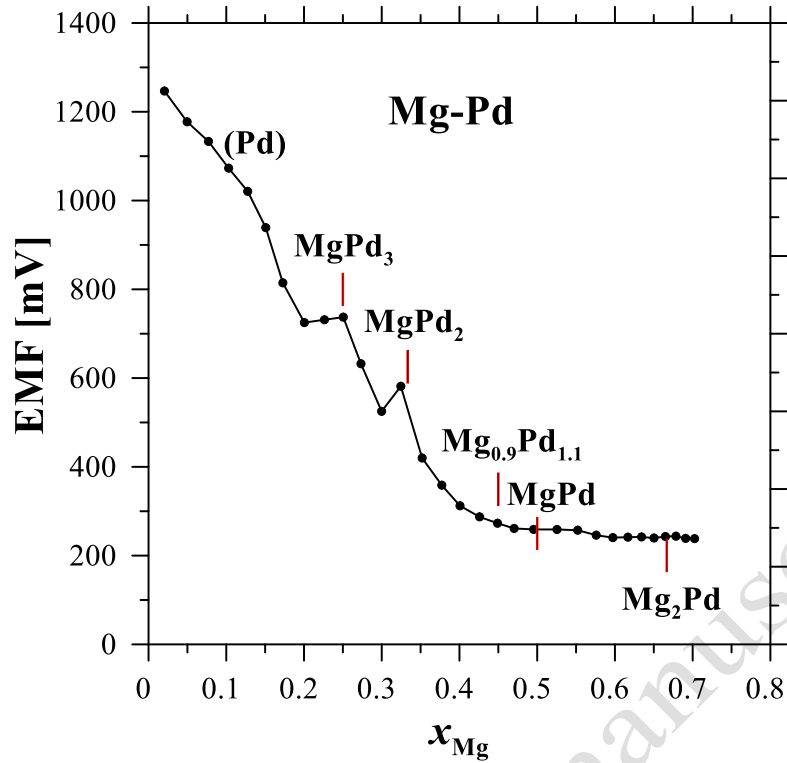
Figure 3. Coulometric titration curve for the Mg-Pd system for measurements made at 918 K.

3.2 Calculation of the Mg-Pd phase diagram

In this work, the following phases were included: Liquid, HCP_A3(Mg), FCC_A1(Pd), Mg_6Pd, $Mg_{306}Pd_{77}$ (ε), $Mg_{785}Pd_{215}$ (ζ), Mg_3Pd (η), Mg_5Pd_2, Mg_2Pd, $MgPd$, $Mg_{0.9}Pd_{1.1}$, $MgPd_2$, and $MgPd_3$. The phases Mg_2Pd_5, as well as Mg_3Pd_5, were omitted in this work due to a lack of information on its thermal stabilities and crystal structures. The absence of this information doesn't allow for thermodynamic modeling or ab initio calculation.

In the beginning, the formation energies at 0 K were recalculated. All the calculations were done using VASP 6.2.1 software [20]. Obtained results compared with literature data are gathered in Table 2 and Figure 4.

Table 2. Formation energies and fusion/decomposition temperatures of intermetallic phases in the Mg-Pd system. The T represents the temperature at which formation energy was determined, the T^f represents the fusion temperature.

Phase	Formation energy [J/mol atom]	T [K]	T^f [K]	Reference
Mg_6Pd	-27864	0	847	This work
	-26100 ±1300	548		[6] exp.

13

	-27000 ÷ -29500	298		[9] exp.
	-24507	0		[11] calc.
Mg_3Pd	-40952	0		This work
	-39945	0		[9] exp.
Mg_5Pd_2	-46047	0	969	This work
	-39500±1600	548		[6] exp.
	-46400 ÷ -47700	298		[9] exp.
	-44769	0		[11] calc.
$MgPd$	-69855	0	1274	This work
	-63388	0		[11] calc.
Mg_3Pd_5	-61466	0		This work
	-59840	0		[11] calc.
	-68080	1073		[8] exp.
$MgPd_2$	-57526	0	899	This work
	-58850	1073		[8] exp.
$MgPd_3$	-46530	0	977	This work
	-45380	1073		[8] exp.
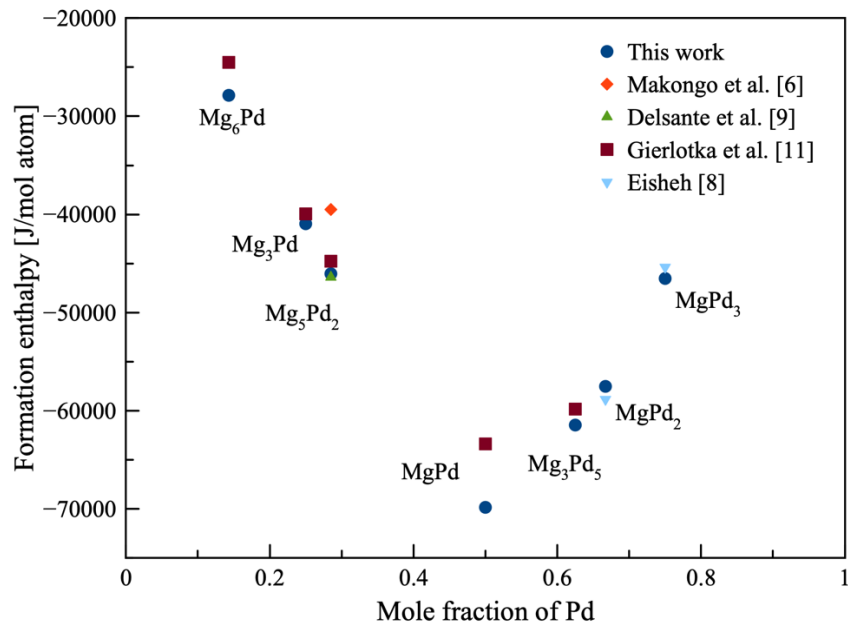
Figure 4. Formation energies of intermediate phases in the Mg-Pd system.

The comparison of calculated enthalpies of formation with literature data reveals a very good agreement between theoretical prediction and experimental data. A bigger discrepancy can be found in the case of our previous calculation and current results for the Mg_6Pd phase. The difference is equal to 3 kJ per mol of atoms which is 13% of its value and it is caused by the application of different pseudopotentials in both series of calculations. However, taking into account a very good agreement of current results with the experimental ones, it is possible to assume that the presented formation enthalpies obtained from ab initio calculations are truthful. Having the formation energies of intermetallic compounds calculated it was possible to repeat the calculations for non-equilibrium positions of atoms in supercells. The supercells were generated by Phonopy [22]. The size of a supercell was adjusted in agreement with the Phonopy [22] guideline that states the size of a lattice constant of the supercell should be bigger than one nanometer. After obtaining a set of data for non-equilibrium atomic positions it was possible to calculate the heat capacity of intermetallic under constant pressure. Figure 5 shows the obtained results.
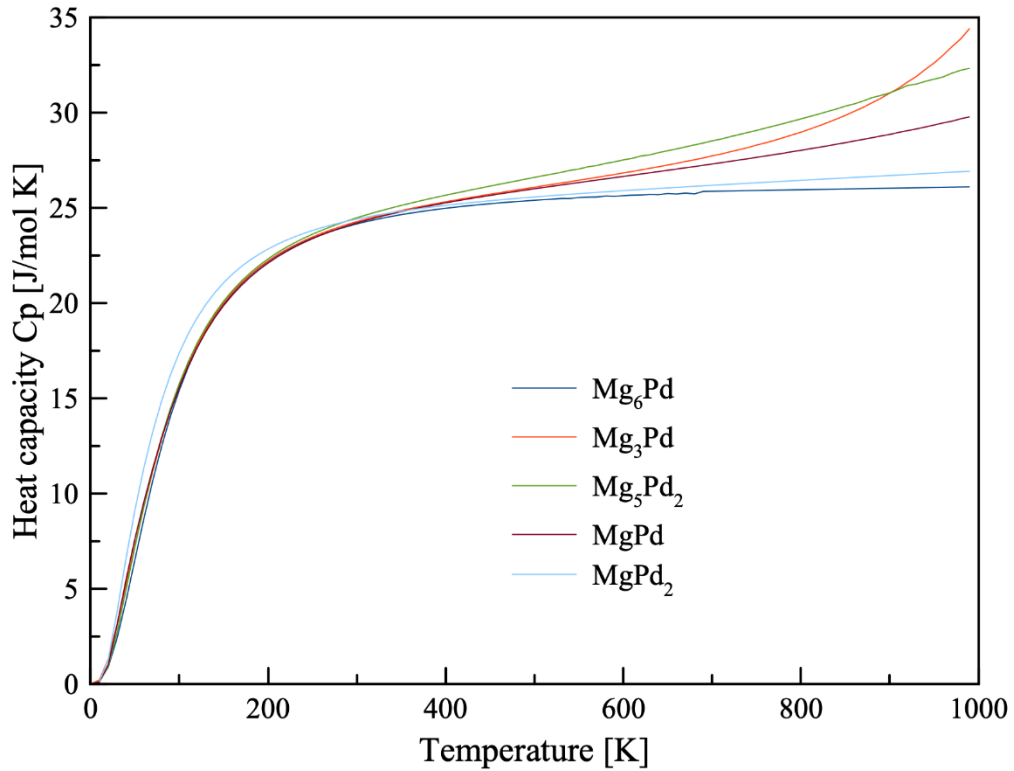
Figure 5. Calculated heat capacities of intermetallic compounds in the Mg-Pd system.

It can be seen that all phases but Mg_3Pd exhibit almost a temperature linear dependency of constant pressure heat capacity at temperatures higher than 300 K. Similar results were obtained in our previous work on the Mg-Pt system [13] where high temperature calculations of heat capacity showed linear dependency on temperature. The obtained results were included in a very poor dataset that was used in the course of thermodynamic optimization. First, the liquid phase was preliminary optimized based on the mixing enthalpy measurements [10]. After that, the information about the liquidus line for the HCP_A3(Mg) was added and the liquid phase was optimized again. As it is easy to notice, all mentioned above data allows for a description of the Mg-rich part of the Mg-Pd system. In the next step of optimization, the Gibbs energies of three following congruently melting phases (Mg_6Pd, Mg_5Pd_2, and Mg_3Pd_5) were added, which Gibbs energies were obtained from the ab inito calculations by applying Phonopy [22] code. This step allowed for the initial optimization of liquid in a whole range of compositions. Following this stage, the thermodynamics of other intermediate phases were

16

determined using the information on heat capacities obtained from ab initio calculations and phase equilibria given by Makongo et al. [6], Eisheh [8], and Delsante et al. [9]. Finally, the thermodynamic description of the FCC_A1 (Pd) phase was assessed. In the last step, all the parameters were optimized to get the best fitting of all available information. All the experimental information were used during optimization with a weight set to be equal to 1. The experimental error was set in agreement with the information provided by the authors of the experimental information. For example, the liquidus data given by Savitskii had to be extracted from a picture, and the experimental error was set to 10 K. On the other hand, Eisheh [8] provided analysis of heating and cooling curves with heating/cooling ratios equal to 20, 10, 5, and 2 deg/min and based on extrapolation of these data to heating/cooling rate equal to 0 deg/min. The analysis of the heating/cooling curves allowed Makongo to propose a value of experimental error equal to 1 K. Similarly, an experimental error equal to 1 degree was given by Delasante et al. for their DSC measurements. Following information given by Makongo et al. [6] and Delasante et al. [9] the 1 K was applied during the optimization procedure. The formation enthalpy of intermetallic compounds was used in the optimization procedure along with experimental errors given by the authors of the investigations. The theoretical prediction of formation enthalpy was given an error equal to 1 kJ/mol of atoms to allow the optimization procedure to work more evenly and not shift toward theoretical prediction. The value of 1 kJ/mole is similar to the experimental error and seems more reasonable than the error of calculation that was equal to c.a. 100 J/mol atom as it was noticed in the description of ab initio calculations. The obtained thermodynamic parameters are gathered in Table 3.

Table 3. Thermodynamic parameters obtained in this work.

Phase	Function [J/mol atom]
Liquid	$^{0}L^{Liquid}_{Mg,Pd} = -194404.3 + 151.2832 * T - 22.4077 * T * \ln(T)$
	$^{1}L^{Liquid}_{Mg,Pd} = -229382.2 + 329.3496 * T - 28.1870 * T * \ln(T)$
	$^{2}L^{Liquid}_{Mg,Pd} = 196138.0 - 82.0331 * T$
FCC_A1	$^{0}L^{FCC\_A1}_{Mg,Pd} = -157684.5 - 16.5046 * T$
	$^{1}L^{FCC\_A1}_{Mg,Pd} = 152447.7 - 96.7427 * T$
Mg$_6$Pd	$^{0}G^{Mg_6Pd}_{Mg:Pd} = -25635.5 - 1.4678 * T + 0.857 * GHSERMG$ $+ 0.143 * GHSERPD$
Mg$_{306}$Pd$_{77}$	$^{0}G^{Mg_{306}Pd_{77}}_{Mg:Pd} = -33590.0 - 2.9948 * T + 0.799 * GHSERMG$ $+ 0.201 * GHSERPD$
Mg$_{785}$Pd$_{215}$	$^{0}G^{Mg_{785}Pd_{512}}_{Mg:Pd} = -35500.0 - 3.1729 * T + 0.785 * GHSERMG$ $+ 0.215 * GHSERPD$
Mg$_3$Pd	$^{0}G^{Mg_3Pd}_{Mg:Pd} = -39900.0 - 3.6185 * T + 0.75 * GHSERMG$ $+ 0.25 * GHSERPD$
Mg$_5$Pd$_2$	$^{0}G^{Mg_5Pd_2}_{Mg:Pd} = -44211.2 - 3.5965 * T + 0.715 * GHSERMG$ $+ 0.285 * GHSERPD$
Mg$_2$Pd	$^{0}G^{Mg_2Pd}_{Mg:Pd} = -49974.3 - 1.6917 * T + 0.667 * GHSERMG$ $+ 0.333 * GHSERPD$
MgPd	$^{0}G^{Mg\ Pd}_{Mg:Pd} = -69855.0 + 4.7568 * T + 0.5 * GHSERMG$ $+ 0.5 * GHSERPD$
Mg$_{0.9}$Pd$_{1.1}$	$^{0}G^{Mg_{0.9}Pd_{1.1}}_{Mg:Pd} = -71000.0 + 3.8954 * T + 0.45 * GHSERMG$ $+ 0.55 * GHSERPD$
MgPd$_2$	$^{0}G^{Mg\ Pd_2}_{Mg:Pd} = -57000.0 + 3.9817 * T + 0.333 * GHSERMG$ $+ 0.667 * GHSERPD$
MgPd$_3$	$^{0}G^{Mg\ Pd_3}_{Mg:Pd} = -47000.0 + 3.9671 * T + 0.25 * GHSERMG$ $+ 0.75 * GHSERPD$

The calculated phase diagram of the binary Mg – Pd phase diagram is shown in Figure 6, together with the experimental liquidus data provided by Makongo et al. [6] Nayeb-Hashemi and Clark [1], and Eisheh [8]. The detailed information on invariant reactions calculated in this work along with experimental determinations are given in Table 4.

18

Table 4. Invariant reactions in the binary Mg-Pd system involved in this work.

Reaction	T [K]	composition			Reference
		x^1_{Pd}	x^2_{Pd}	x^3_{Pd}	
$L \rightleftharpoons HCP\_A3 + Mg_6Pd$	807	0.099	0.000	0.143	This work
	813	~0.078	-	-	[1]
	813±10	~0.080	~0.02	-	[2]
$L \rightleftharpoons Mg_6Pd + Mg_{306}Pd_{77}$	817	0.174	0.143	0.201	This work
$L + Mg_{785}Pd_{215} \rightleftharpoons Mg_{306}Pd_{77}$	842	0.197	0.215	0.201	This work
	838	-	0.215	0.201	[6]
$L \rightleftharpoons Mg_{785}Pd_{215} + Mg_3Pd$	855	0.216	0.215	0.250	This work
	853	-	0.215	0.250	[6]
$L + Mg_5Pd_2 \rightleftharpoons Mg_3Pd$	899	0.240	0.285	0.250	This work
	898	-	0.285	0.250	[6]
$L \rightleftharpoons Mg_5Pd_2 + MgPd$	961	0.304	0.285	0.500	This work
	963	~0.32	0.285	-	[6]
$L + Mg_{0.9}Pd_{1.1} \rightleftharpoons MgPd$	1276	0.371	0.550	0.500	This work
	1276	-	-	-	[6]
$L \rightleftharpoons Mg_{0.9}Pd_{1.1} + FCC\_A1$	1541	0.658	0.550	0.778	This work
	1553	0.637	0.550	-	[2]
$Mg_5Pd_2 + MgPd \rightleftharpoons Mg_2Pd$	952	0.285	0.500	0.333	This work
	954	0.285	0.500	0.333	[6]
$Mg_{0.9}Pd_{1.1} + FCC\_A1 \rightleftharpoons MgPd_3$	977	0.550	0.807	0.750	This work
	977	0.658	0.820	0.750	[8]
$Mg_{0.9}Pd_{1.1} + MgPd_3 \rightleftharpoons MgPd_2$	902	0.550	0.750	0.667	This work
	901	0.685	0.750	0.667	[8]

It can be seen that the calculated invariant reactions reproduced well experimental information given by Makongo et al. [6], Nayeb-Hashemi and Clark [1], and Eisheh [8]. The difference between the model and experiment slightly exceeds the experimental errors given by the authors of the investigations [8], [6]. It is believed that further experimental works on phase equilibria and thermodynamic properties will allow for improvement of the thermodynamic description of the Mg-Pd system.

The Mg-rich part of the calculated phase diagram follows Makongo et al. [6] proposition of phase equilibria. The tricky part of the phase diagram assessment was to make a critical evaluation of all available data for the Pd-rich part of the phase diagram. Although Makongo et al. [6] drew the $Mg_{0.9}Pd_{1.1}$ phase, they didn't determine it from the experiment, similar to Eisheh [8] who also did not determine that phase. Instead of this, Eisheh [8] proposed a Mg_3Pd phase as a neighbor phase to the MgPd compound. Moreover, in his work, two phases, $MgPd_2$ and $MgPd_3$, that decompose by peritectic reactions at 901 K and 977 K, respectively, as well as the Mg_2Pd_5 phase were suggested. Since there is no further information about the thermal stability and the crystal structure of the Mg_2Pd_5, in our work this compound was omitted, because it would be impossible to calculate its Gibbs energy from ab initio supported by phonon dispersion. One can see that the calculated phase diagram agrees well with the experimental data given by Makongo et al. [6]. The liquidus line for a concentration of palladium between 0.15 and 0.25 mole fraction is reproduced fair. The calculated Mg solubility in Pd shows reasonable agreement with experimental data reported by Eisheh [8]. Increasing solubility of Mg in Pd causes the unwanted appearance of this phase in the Mg-rich part of the Mg-Pd phase diagram. The problem can have a source in the stability of Mg in the FCC structure applied in this work. According to the SGTE Database [29], the difference between HCP and FCC is equal to 2600 J/mol at 0 K; however, the ab initio calculation shows a difference between these crystal structures equal to 2894 J/mol. It is guessed that the application of the more positive energy of the Mg in the FCC_A1 would resolve the unwanted appearance of FCC_A1 in the Mg-rich side

of the phase diagram. However, keeping the description in agreement with the SGTE database [29] does not allow for any modification of Gibbs energies of pure elements (Mg, Pd).
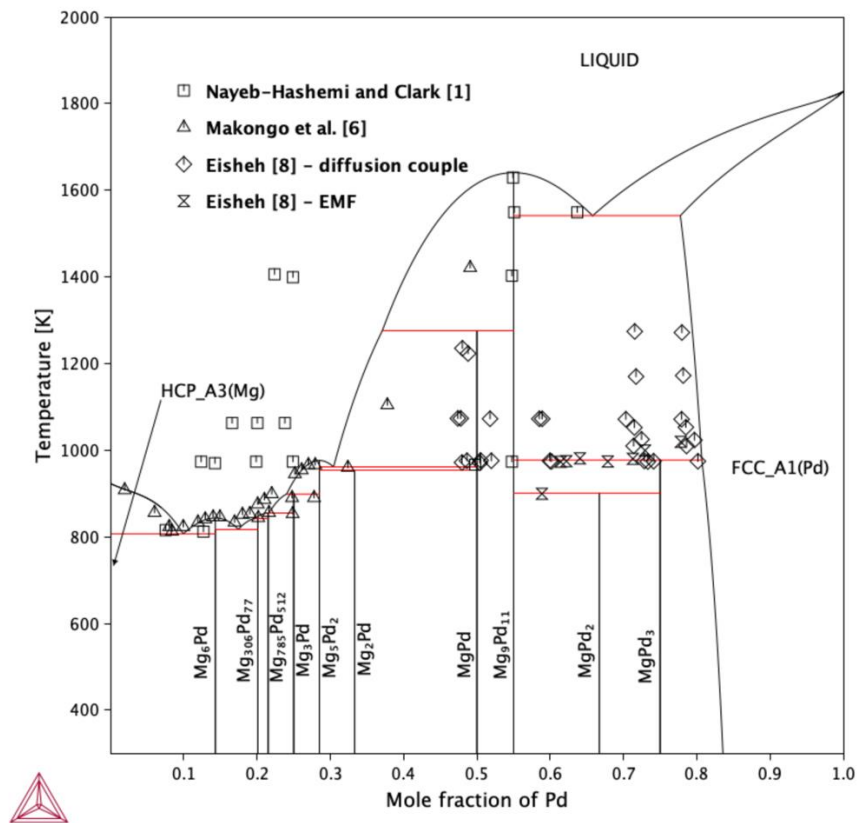
Figure 6. Calculated phase diagram superimposed with experimental data given by [1] [6] [8].

It can also be noticed that information on the Mg-Pd phase diagram reported by Nayeb-Hashemi and Clark [1] does not agree with the data given by Makongo et al. [6]. Regardless of the different intermediate phases listed by both sources, the liquidus temperature varies significantly with a difference of about 200 degrees for low concentrations of Pd. It is then obvious that further investigations on solid and liquid phases of the Mg-Pd system are necessary.

The phase diagram obtained shows that the electrochemical tests performed were carried out entirely in the solid range. It can be seen a quite good agreement between the calculations and results from titration in the Mg-Pd system for characteristic changes within the intermetallic phases. Therefore, this result may be treated as proof of the correct selection of stoichiometry of IMCs included in the optimization.

Figure 7 shows the calculated enthalpy of the mixing of the liquid phase at 1116 K, 1031 K, and 990 K together with experimental data obtained by Dębski et al. [10]. It can be seen that the modeled enthalpy of mixing reproduces experimental data pretty well and that the experimental determination of mixing enthalpy shows slight temperature dependency. The modeled mixing enthalpy of the liquid phase exhibits dual characteristics: for a low concentration of palladium, the mixing enthalpy is negative, whereas for the concentration of Pd greater than 0.7 mole fraction it shows positive values.
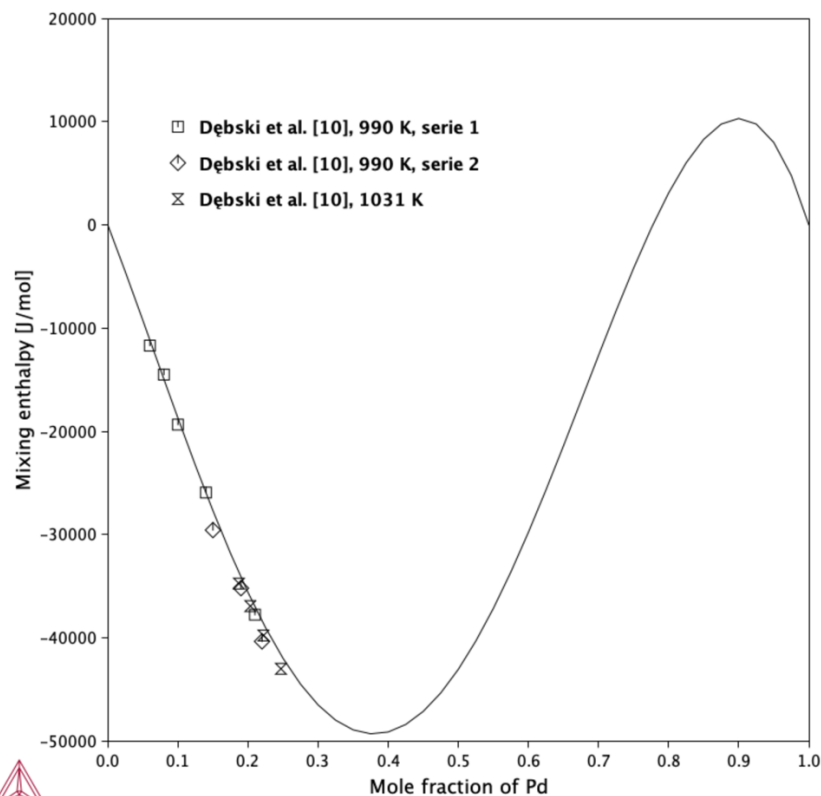
Figure 7. Calculated enthalpy of mixing of liquid Mg-Pd at 990 K superimposed with experimental data given by Dębski et al. [10] and obtained in this work.

It can be noticed that the s-shape of mixing enthalpy varies from the one proposed by Dębski et al. [8] in their work. Application of the negative heat of mixing for a whole range of compositions leads to unresolvable problems with the assessment of the FCC_A1 (Pd) phase. It is believed that experimental investigations on thermodynamic properties of the liquid phase that covers the Pd-rich region will clearly show the characteristics of the heat of mixing.

Moreover, although the experimental data given by Dębski et al. [10] doesn't show a clear temperature dependency, what will justify using the term c*T*ln(T) in the description of liquid phase; however, without this term optimization was not successful. It can be stated again that only thermodynamic investigations on mixing enthalpy and activities of components in a whole composition range will bring a clear answer to the above doubts.

4 Conclusions

The thermodynamic investigation and phase diagram calculations of the magnesium-palladium system were inspired by the possible use of these alloys as potential hydrogen storage materials.

The proposed in this work the Mg-Pd phase diagram together with the complete optimized thermodynamic parameters is the first thermodynamic assessment in the literature.

For the optimization of the thermodynamic properties of phases, available experimental information as well as ab initio calculations were used.

The application of phonon dispersion calculations allowed for the determination of the heat capacity of intermetallic compounds with known crystal structures.

Although the proposed phase diagram seems to be consistent with the majority of literature information, further investigations on the phase equilibria and thermodynamics of liquid and solid Mg-Pd solutions are necessary and justified.

Especially valuable will be experiments concerned with the calorimetric and activity determination of the mixing enthalpy change for liquid and solid solutions of the high concentration of Pd, as well as the activity of Mg and/or Pd. Due to the high vapor pressure of Mg, it seems that the vapor pressure measurements should be applied to achieve this goal.

The obtained thermodynamic description can be used in various applications and different types of materials.

23

Declaration of Competing Interests

The authors declare that they have no known competing financial interests or personal relationships that could have appeared to influence the work reported in this paper.

References:

[1] A. Nayeb-Hashemi and J. Clark, "The Mg−Pd (magnesium-palladium) system," *Bulletin of Alloy Phase Diagrams,* vol. 6, pp. 164-167, 1985.

[2] E. Savitsky, V. Terekhova and N. Birun, "Equilibrium Diagram of the Mg−Pd System," *Russian Journal of Inorganic Chemistry,* vol. 7, pp. 1228-1231, 1962.

[3] R. Ferro and G. Rambaldi, "Research on the alloys of noble metals with the more electropositive elements: III. Micrographic and X-ray examination of some magnesium-platinum alloys," *Journal of the Less-Copmmon Metals,* vol. 2, pp. 383-391, 1960.

[4] L. Westen, "A Palladium-Magnesium Alloy Phase of Al_5Co_2 Type," *Acta Chemica Scandinavia,* vol. 22, pp. 2574-2580, 1968.

[5] P. I. Kripyakievich and E. I. Gladyshevskii, "Crystal Structures of Some Compounds of Palladium with Magnesium," *Kristallografiya,* vol. 5, pp. 577-579, 1960.

[6] J. P. A. Makongo, Y. Prots, U. Burkhardt, R. Niewa, C. Kudla and G. Kreiner, "A case study of complex metallic alloy phases: structure and disorder phenomena of Mg-Pd compounds," *Philosophical Magazine,* vol. 86, pp. 427-433, 2006.

[7] H. Okamoto, "Mg-Pd (Magnesium-Palladium)," *Journal of Phase Equilibria and Diffusion,* vol. 31, pp. 407-408, 2010.

[8] J.-T. Eisheh, *PhD Dissertation: Investigations on the thermodynamics, constitution and diffusion of the magnesium-platinum and magnesium-palladium systems,* Kiel: Christian-Albrechts-Universitat zu Kiel, 2006.

[9] S. Delsante, R. Novakovic, A. Gagliolo and G. Borzone, "Thermodynamic investigation on the Mg-Pd intermetallic phases," *Journal of Chemical Thermodynamics,* vol. 139, p. 105890, 2019.

[10] A. Dębski, S. Terlicka, W. Gąsior, W. Gierlotka, M. Pęska and M. Polański, "Thermodynamic properties of Mg-Pd liquid alloys," *Journal of Molecular Liquids,* vol. 317, p. 114024, 2020.

[11] W. Gierlotka, A. Dębski, S. Terlicka, W. Gąsior, M. Pęska and M. Polański, "Insight into Phase Stability in the Mg-Pd System: The Ab Initio Calculations," *Journal of Phase Equilibria and Diffusion*, vol. 41, pp. 681–686, 2020.

[12] A. Dębski, S. Terlicka, W. Gąsior, W. Gierlotka, M. Pęska, J. Dworecka-Wójcik and M. Polański, "Calorimetric Studies of Magnesium-Rich Mg-Pd Alloys," *Materials,* vol. 14, pp. 680-689, 2021.

[13] W. Gierlotka, A. Dębski, S. Terlicka, W. Gąsior, M. Pęska, J. Dworecka-Wójcik and M. Polański, "Theoretical studies of the thermodynamic and mechanical properties of Mg–Pt system. An insight into phase equilibria," *Journal of Materials Research,* vol. 37, pp. 1904–1915, 2022.

[14] R. A. Huggins, "Principles determining the potentials and capacitioes of electrochemical cells," in *C. Julien, Z. Stoynov, Materials for Lithium-Ion Batteries*, Doprdrecht, Springer, 2000.

[15] W. Weppner and R. Huggins, "Thermodynamic properties of the intermetallic systems lithium-antimony and lithium-bismuth," *Joutnal of Electrochemical Society,* vol. 125, pp. 7-14, 1978.

[16] J. Wang, P. King and R. Huggins, "Investigations of binary lithium-zinc, lithium-cadmium and lithium-lead alloys as negative electrodes in organic solvent-based electrolyte," *Solid State Ionics,* vol. 20, pp. 185-189, 1986.

[17] W. Plieth, "Chapter 3: El;ectrode Potentials," in *Electrochemistry for Materials Science*, Elsevier Science, 2008.

[18] M. E. Trybula, S. Terlicka and P. Fima, "Thermodynamics of liquid Li-Sb alloys – Experiment vs modeling," *Journal of Chemical Thermodynamics,* vol. 128, pp. 134-140, 2019.

[19] W. Gąsior, Z. Moser and W. Zakulski, "Thermodynamoic studies and the phase dioagram of the Li-Sn system," *Journal of the Non-Crystalline Solids,* vol. 205-207, pp. 379-382, 1996.

[20] G. Kresse and J. Hafner, "Ab initio molecular dynamics for liquid metals," *Physical Review B,* vol. 47, p. 558, 1993.

[21] J. P. Perdew, K. Burke and M. Ernzernhof, "Generalized Gradient Approximation Made Simple," *Phys. Rev. Lett.,* vol. 77, p. 3865, 1996.

[22] A. Togo and I. Tanaka, "First principle phonon calculations," *Scripta Materialia,* vol. 108, pp. 1-5, 2015.

[23] W. H. Press, S. A. Flannery, S. A. Teukolsky and W. T. Vetterling, Numerical Recipes, New York: Cambridge University Press, 1986.

[24] F. I. Mopsik, "The Quasi-Harmonic Approximation and Generalized Gruneisen Equation of State," *Journal of Research of the National Bureau of Standards - A. Physics and Chemistry,* vol. 77A, pp. 407-409, 1973.

[25] L. Kaufman and H. Bernstein, Computer calculation of phase diagrams. With special reference to refractory metals, New York: Academic Press Inc., 1970.

[26] W. Gierlotka, "Thermodyunamic assessment of the Ag-Te binary system," *Journal of Alloys and Compounds,* vol. 485, pp. 231-235, 2009.

[27] H. J. Wu, W. J. Foo, W. Gierlotka, S. W. Chen and G. J. Snyder, "The microstructure, liquidus projection and thermodynamic modeling of thermoelectric Ag-Pb-Te system," *Materials Chemistry and Physics,* vol. 141, pp. 758-767, 2013.

[28] W. Gierlotka, J. Łapsa and D. Jendrzejczyk, "Thermodynamic description of the Pb-Te system using ionic liquid model," *Journal of Alloys and Compounds,* vol. 479, pp. 152-156, 2009.

[29] Scientific Group Thermodata Europe, *Unary Thermodynamics Database,* 2015.